Monthly Notices
of the
ROYAL ASTRONOMICAL SOCIETY

MNRAS **469,** 1532–1544 (2017)
Advance Access publication 2017 April 21

doi:10.1093/mnras/stx927

On the impact of helium abundance on the Cepheid period–luminosity and Wesenheit relations and the distance ladder

R. Carini,[1]★ E. Brocato,[1] G. Raimondo[2] and M. Marconi[3]

[1]*INAF–Osservatorio Astronomico di Roma, via Frascati 33, I-00078 Monte Porzio Catone, Italy*
[2]*INAF–Osservatorio Astronomico di Teramo, Mentore Maggini s.n.c., I-64100 Teramo, Italy*
[3]*INAF–Osservatorio Astronomico di Capodimonte, Salita Moiariello 16, I-80131 Napoli, Italy*

Accepted 2017 April 12. Received 2017 April 5; in original form 2016 June 24

ABSTRACT

This work analyses the effect of the helium content on synthetic period–luminosity relations (PLRs) and period–Wesenheit relations (PWRs) of Cepheids and the systematic uncertainties on the derived distances that a hidden population of He-enhanced Cepheids may generate. We use new stellar and pulsation models to build a homogeneous and consistent framework to derive the Cepheid features. The Cepheid populations expected in synthetic colour–magnitude diagrams of young stellar systems (from 20 to 250 Myr) are computed in several photometric bands for $Y = 0.25$ and 0.35, at a fixed metallicity ($Z = 0.008$). The PLRs appear to be very similar in the two cases, with negligible effects (few per cent) on distances, while PWRs differ somewhat, with systematic uncertainties in deriving distances as high as ~ 7 per cent at $\log P < 1.5$. Statistical effects due to the number of variables used to determine the relations contribute to a distance systematic error of the order of few percent, with values decreasing from optical to near-infrared bands. The empirical PWRs derived from multiwavelength data sets for the Large Magellanic Cloud (LMC) is in a very good agreement with our theoretical PWRs obtained with a standard He content, supporting the evidence that LMC Cepheids do not show any He effect.

Key words: stars: abundances – stars: variables: Cepheids – distance scale.

INTRODUCTION

Through the period–luminosity relations (PLRs), classical Cepheids are fundamental standard candles for the calibration of secondary distance indicators (as Supernovae Ia, surface brightness fluctuations, etc.), for the determination of the cosmological distances and the Hubble constant (Freedman et al. 2001; Saha et al. 2001). In spite of this, the general question of the dependence of the Cepheid properties and consequently their PLRs on the chemical composition, discussed by many authors over the years, still lacks of firm conclusions, and the size and even the sign of the effects are still disputed (see e.g. Sasselov et al. 1997; Kennicutt et al. 1998; Bono, Marconi & Stellingwerf 1999a; Fiorentino et al. 2002; Storm et al. 2004; Marconi, Musella & Fiorentino 2005; Romaniello et al. 2008; Freedman & Madore 2010; Efstathiou 2014).

In particular, the effect of He abundance on Cepheid pulsation properties has been theoretically investigated by Bono et al. (2000), Fiorentino et al. (2002) and Marconi et al. (2005) for $Z \geq 0.02$. At fixed metallicity, an increase in the He content produces a shift towards higher effective temperature. If both the metallicity and the He abundances increase, as expected, the two effects on the instability-strip topology tend to compensate each other. Moreover, at fixed He to metal enrichment ratio ($\Delta Y/\Delta Z$), as the metallicity increases from $Z = 0.03$ to 0.04, the instability strip tends to narrow. As a result of the complex interplay between He and metal variations, in the case of metal-rich ($Z \geq 0.01$) Cepheid samples, the predicted correction for metallicity to the Large Magellanic Cloud (LMC)-based PLR was found to be dependent on the assumed $\Delta Y/\Delta Z$ (see Fiorentino et al. 2002 and Marconi et al. 2005 for details) and to show an opposite sign when comparing Milky Way (MW) and Magellanic Clouds Cepheids in agreement with Romaniello et al. (2008). To reduce the influence of the instability-strip topology and of the contribution of metals, the period–Wesenheit relations (PWRs; Madore 1982) are often adopted. These relations have the additional advantage of widely removing the reddening effect and of significantly reducing the dispersion of visual magnitudes at a given period. In fact, the dispersion of the PWRs for the LMC Cepheids is 2÷3 times smaller compared to the optical PLRs (Tanvir 1999; Udalski et al. 1999; Fouqué et al. 2007; Soszynski et al. 2008; Ngeow et al. 2009). This reduces the random errors in the evaluation of distances. It is worth noting that the PWRs rely on the assumed extinction law, and any deviation of the extinction coefficients could introduce systematic errors on the inferred distances,

★ E-mail: roberta.carini@oa-roma.inaf.it

with major impact in star forming regions, like 30 Doradus (see e.g. De Marchi et al. 2016). The effect of variations in the He content on the PWRs has been predicted by Carini et al. (2014) at the LMC typical metal content ($Z \simeq 0.008$). In that paper, we showed that, at fixed metallicity, the instability strip of fundamental pulsators becomes hotter when the He increases from the standard value $Y = 0.25$ to 0.35. At fixed mass, Cepheids with higher He abundance pulsate with longer periods and, consequently, the PWRs have different slopes with respect to those of standard relations, as shown in fig. 10 and table 5 in Carini et al. (2014). In this paper, we analyse the effect of He content on synthetic PLRs and PWRs and on the inferred Cepheid-based distance determinations, by relying on stellar pulsation, stellar evolution and population synthesis models. We explore the role He-enhanced Cepheids might have if present in a sizable fraction. In particular, we will verify whether and how the PLRs and PWRs may be affected by the presence of Cepheids with non-standard He contents, through comparisons with samples of Cepheids observed in the LMC. This has relevant implications in view of the present efforts to reach the 1 per cent level to properly confront the local value of H_0 with the microwave background measurements.

Moreover, it is now well known that multiple stellar populations are present in the globular clusters (GCs) of the MW (see the review by Piotto 2009), where the chemistry of stars belonging to the second generation(s) (SG) is altered with respect to the abundances of the original gas from which the cluster has been formed (Gratton, Sneden & Carretta 2004; Carretta et al. 2009a; Gratton, Carretta & Bragaglia 2012). Some studies suggested that the newly formed stars should be He-enhanced (up to $Y \sim 0.40$; e.g. Piotto et al. 2007; Gratton et al. 2010; Marino et al. 2014), while their metallicity appears nearly constant (the differences are less than 0.05 dex; Carretta et al. 2009b). Such an evidence seems to favour the hypothesis that the progenitors of the GCs with MPs should be very massive ($M > 10^5$ $M_\odot$), with SG stars formed during the first ∼150 million years of the cluster's life (Decressin, Charbonnel & Meynet 2007; D'Ercole et al. 2008; de Mink et al. 2009; Bastian et al. 2013). If a similar formation history is assumed, one expects signatures of SG stars in (relatively) young massive clusters. For instance, Cepheids with different chemical content (with respect to the bulk of stars) might exist as well, even if to date they have not been detected. He-enhanced variables in observed samples of Cepheids could, in principle, alter the slope and zero-point of PLRs and PWRs, with respect to those derived from He-standard variables. Unfortunately, observations available up to now do not support or exclude in a conclusive way the presence of SG He-enhanced stars in young stellar systems. Some intermediate-age (∼ 1–2 Gyr) clusters of the LMC show distinct main-sequence (MS) turn-offs, as well as few younger clusters (Milone et al. 2016). This occurrence has been interpreted as a sign of (at least) two main episodes of star formation, although alternative explanations have been invoked (different rotation rates, binaries, etc., e.g. Milone et al. 2009, 2017). The picture is still uncompleted and deserve more investigations using different approaches. In this paper, we make a theoretical investigation to explore the impact of multiple populations with different He content on the observed Cepheids properties of a stellar system.

The paper is arranged as follows. Section 1 describes the stellar evolution and pulsation models and introduces the adopted stellar population synthesis models. Our theoretical PL and PW relations for the two values of initial He are compared with the most updated empirical ones derived from multiwavelength data sets for the LMC in Section 2. In Section 3, our theoretical results are compared to Cepheids in LMC adopting OGLE III (Soszynski et al. 2008; Udalski et al. 2008) and VMC (Cioni et al. 2011; Ripepi et al. 2012) releases. In Section 4, we evaluate the stochastic effects on deriving distances when only a small sample (∼50) of Cepheids is available. A brief discussion closes the paper.

1 MODEL COMPUTATIONS

1.1 Stellar evolution and pulsation models

Stellar evolution models have been computed using the ATON evolutionary code (Ventura et al. 1998) and published in Carini et al. (2014). Here, we briefly recall the main assumptions of the code. The convective instability is described by means of the full spectrum of turbulence (FST) model developed by Canuto & Mazzitelli (1991); the mass-loss rate in the ATON case is determined via the Blöcker's formulation (Blöcker 1995):

$$\dot{M} = 4.83 \times 10^{-22} \eta_R M^{-3.1} L^{3.7} R,$$

where M, L and R are denoted in solar units, η_R is a free parameter. We used $\eta_R = 0.02$.

The mixing of chemicals and nuclear burning is coupled with a diffusive approach, according to the scheme suggested by Cloutman & Eoll (1976). The overshoot of convective eddies into radiatively stable regions is described by an exponential decay of the velocity beyond the formal border found via the Schwarzschild criterion. The extent of the overshoot is given by the free parameter ξ; in this study, we put $\xi = 0.02$ in agreement with the calibration given in Ventura et al. (1998). No overshooting is used for the evolutionary phases following the core He-burning phase.

The evolutionary models used in this work have metallicity $Z = 0.008$, initial He $Y = 0.25$ and $Y = 0.35$; the mixture is α-enhanced, with [α/Fe]=+0.2, with the reference solar mixture taken from Grevesse & Sauval (1998). The star evolution with both He contents is followed from the MS to the beginning of the phase of thermal pulses; the range in mass is from 0.4 $M_\odot$ to 12 $M_\odot$.

The sets of pulsation models computed for the above chemical compositions in Carini et al. (2014) have been extended with the computation of a finer grid of stellar masses with the same non-linear pulsation code (see Marconi et al. 2005, 2010 and references therein). The adopted physical and numerical assumptions are the same as in Marconi et al. (2005, see also Bono, Caputo & Marconi 1998; Bono et al. 1999a for details). Here, we only remind that the adopted non-linear hydrodynamical code includes a non-local time-dependent treatment of convection (Stellingwerf 1982; Bono et al. 1999a). For each adopted stellar mass ranging from 3 $M_\odot$ to 12 $M_\odot$, the assumed luminosity level is based on a canonical mass–luminosity relation (Bono et al. 2000). A wide range of effective temperatures is explored with a step of 100 K in order to investigate the pulsation stability in both the fundamental (F) and the first overtone (FO) mode for each mass, luminosity and chemical composition. More details can be found in Carini et al. (2014).

1.2 Stellar population models

To simulate the properties of stellar populations and of synthetic Cepheids, we used the stellar population synthesis code SPoT, described in Brocato et al. (1999), Brocato et al. (2000), Raimondo et al. (2005) and Raimondo (2009). Here, we recall that the code starts directly from stellar evolutionary tracks and relies on the Monte Carlo techniques for populating the initial mass function (IMF). Since our purpose is to have a reasonable number of variables in the instability strip, we simulated only stars with mass

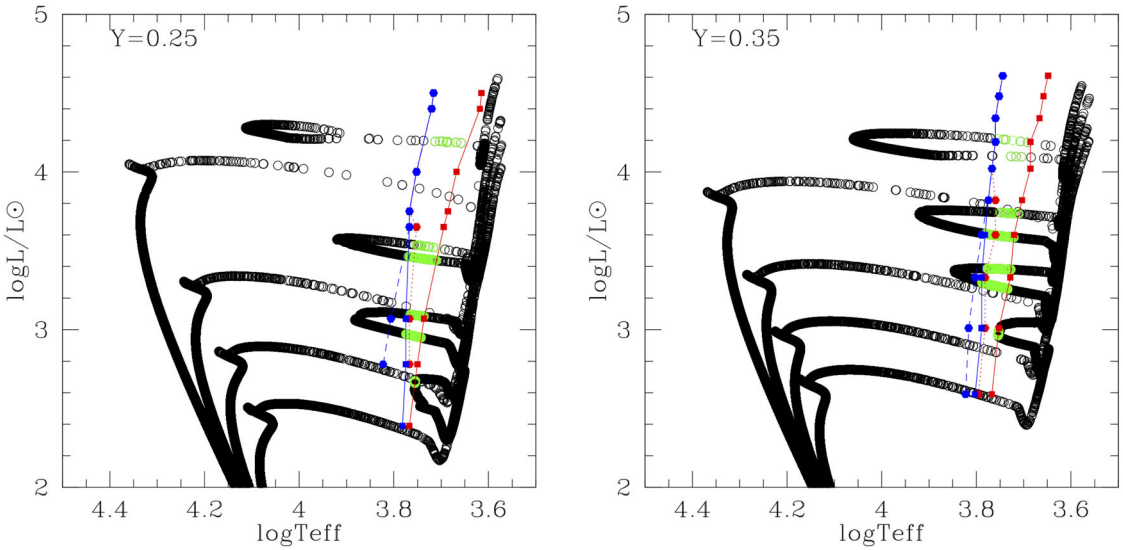

Figure 1. HR diagram of stars populations with $t = 30$, 80, 150 and 254 Myr for $Y = 0.25$ (left-hand panel) and $t = 30$, 60, 100 and 156 Myr for $Y = 0.35$ (right-hand panel). The FRE (solid red line), FORE (dotted red line), FBE (solid blue line) and the FOBE (short dashed blue line) are also shown. In these plots, the photometric uncertainties are neglected. (For a colour version of the figure, see the electronic version of the paper.)

greater than 1 $M_\odot$ and assumed a Salpeter IMF (Salpeter 1955) with exponent $\alpha = 2.35$. The cut at low-mass stars does not affect the conclusions of this paper because we are interested to bright high-mass stars evolving off the MS. All the evolutionary phases, from the MS up to the asymptotic giant branch, are covered by models. For each set of simple stellar population (SSP) parameters (i.e. age, t; metallicity, Z; and He abundance, Y), 100 independent simulations each containing 5000 stars (in the mass range 1–12 $M_\odot$) are computed. Each single simulation corresponds to a stellar population having a total mass of the order of $\sim 10^4$ $M_\odot$, including low-mass stars down to 0.1 $M_\odot$.

We computed synthetic magnitudes and colours (in the U, B, V, R, I, J, H and K bandpasses) by adopting Castelli & Kurucz (2003) stellar atmospheres library. The code has been implemented by including specific routines to compute the number of predicted Cepheids and, for each variable, the pulsation mode and period (Carini et al. 2014). For populations with $Y = 0.25$, we adopted the instability strip calculated by Bono et al. (1999a) and Bono et al. (2001); for $Y = 0.35$, we used the values published in Carini et al. (2014). We consider ages from 20 Myr up to about 250 Myr (with an age step of ∼2 Myr up to 50 Myr, and ∼10 Myr up to 250 Myr) for the first stellar generation ($Y = 0.25$), and from 20 Myr up to 150 Myr (with the same age steps) for Cepheids belonging to the SG of stars ($Y = 0.35$). For older ages, no Cepheids are found in the populations (see Fig. 1). The age steps are chosen to reproduce in detail the main features of the Cepheid populations as a function of the age. The mean mass, luminosity and effective temperature of the stars at the termination of the MS luminosity function, for each population, are listed in Table 1.

In Fig. 1, we present the brightest part of the Hertzsprung–Russel (HR) diagrams expected from a sample of stellar populations having He abundances $Y = 0.25$ (left-hand panel) and $Y = 0.35$ (right-hand panel) and selected ages. The number of stars in each synthetic model shown in Fig. 1 is quite high to ensure that the He-burning phase is well populated also when computing very young stellar populations. This is obtained by collecting together all the 100 independent simulations, in this way each plotted model represents a single burst stellar population with a mass of $\sim 10^6$ $M_\odot$. The instability strips derived from the pulsation models are also plotted: the blue short-dashed line is the first overtone blue edge (FOBE), the blue solid line is the fundamental blue edge (FBE), the red dotted line is the first overtone red edge (FORE) and the red solid line is the fundamental red edge (FRE). Green circles are the stars predicted to be variables.

Within the theoretical framework described in the previous sections, we are able to put constraints on the oldest stellar populations where Cepheids can be observed. In the case of $Y = 0.25$ (left-hand panel), the oldest synthetic population expected to host Cepheids is found to be 254 Myr old, while for $Y = 0.35$ (right-hand panel) the Cepheids should not be observed for ages older than 156 Myr. The exact age values are obtained by computing synthetic models with a very narrow step in age. The difference in the age limits is due to the fact that stars with a high He abundance, due to the higher molecular weight, evolve in a shorter time and are more luminous and hotter than stars with a lower He abundance at fixed mass. Therefore, the population with $Y = 0.35$ and age $t \sim 150$ Myr contains stars with mass lower than ~ 3 $M_\odot$ as well as a population with age ∼250 Myr but with $Y = 0.25$ (Table 2). The reason for the age limits is well known. In old population, the hotter extremity of the blue loop of the evolving stars becomes cold enough to lie outside of the instability strip, so that no star falls inside the instability strip and no Cepheid is foreseen, as clearly shown in Fig. 1. This implies that there are no Cepheids with $Y = 0.35$ pulsating in the fundamental mode with $\log P \lesssim 0.50$ and no Cepheids with $Y = 0.25$ at $\log P \lesssim 0.2$. In Table 2, we report the maximum age of the stellar system hosting Cepheids and the physical properties of pulsating stars, namely mass, luminosity, temperature and period for the two analysed He contents.

We point out that our results depend on the evolutionary scenario we have adopted. Different assumptions concerning the surface boundary condition, solar calibrated mixing length, model of convection, chemical composition, equation of state (EOS), gravitational settling, mass loss and other physics, may result in differences in the evolutionary path in the HR diagram. To throw some light

Table 1. Mean value of the mass, luminosity and temperature of the stars at the termination of the MS luminosity function for each age.

t (Myr)	$M/M_\odot$	$\log L/L_\odot$	$\log T_{\rm eff}$
	$Z = 0.008$ $Y = 0.25$		
22	10.90	4.23	4.35
24	10.34	4.15	4.34
26.5	9.73	4.07	4.33
28	9.40	4.02	4.32
30	9.04	3.97	4.31
35	8.30	3.84	4.29
40	7.74	3.74	4.28
45	7.26	3.64	4.26
50	6.88	3.56	4.25
60	6.28	3.42	4.23
70	5.84	3.31	4.21
80	5.49	3.21	4.20
90	5.20	3.13	4.18
100	4.95	3.05	4.17
110	4.75	2.99	4.16
120	4.56	2.92	4.15
130	4.41	2.87	4.14
140	4.27	2.81	4.13
150	4.15	2.77	4.12
160	4.02	2.71	4.11
170	3.93	2.68	4.10
180	3.84	2.64	4.10
190	3.75	2.60	4.09
200	3.66	2.56	4.09
210	3.60	2.53	4.08
220	3.52	2.50	4.07
230	3.46	2.46	4.07
240	3.39	2.43	4.06
250	3.34	2.41	4.06
	$Z = 0.008$ $Y = 0.35$		
20	8.97	4.11	4.36
22	8.46	4.02	4.35
24	8.03	3.95	4.34
28	7.38	3.83	4.32
30	7.10	3.77	4.32
35	6.53	3.65	4.30
40	6.09	3.54	4.28
45	5.75	3.46	4.26
50	5.46	3.38	4.25
60	4.99	3.24	4.23
70	4.65	3.13	4.21
80	4.37	3.03	4.20
90	4.15	2.95	4.18
100	3.96	2.88	4.17
110	3.80	2.81	4.16
120	3.66	2.75	4.15
130	3.54	2.69	4.14
140	3.43	2.65	4.13
150	3.34	2.60	4.12

Table 2. Mean values for key quantities of variables in the oldest stellar population where Cepheids are expected for the two He contents.

Y	t (Myr)	$M/M_\odot$	$\log L/L_\odot$	$\log T_{\rm eff}$	$\log P$
0.25	254	3.60	2.67	3.76	0.28
0.35	156	3.56	2.97	3.75	0.57

on this point, in Fig. 2, we compare our tracks (solid black lines) with the ones from other popular data bases: the Padova data base[1] (short dashed red lines, $Z = 0.008$, $Y = 0.26$, 0.34), and the Basti data base[2] (long dashed blue lines, $Z = 0.008$, $Y = 0.256$; see Pietrinferni et al. 2004, 2006; Bertelli et al. 2009, for details). We outlight that the Z and Y values are not exactly the same, but are chosen as similar as possible, when available. In Fig. 2, we plot the evolutionary tracks for models of 4 $M_\odot$ and 8 $M_\odot$, for the labelled He abundance values. The black vertical lines represent the instability strip boundaries.

First, we can see that the effect of He abundance is fairly similar in our and Padova tracks. The ATON (black) He-rich 4 $M_\odot$ model is more luminous of ∼0.2 dex at the TO and of ∼0.3 dex at the He-burning loop than the standard one; for the 8 $M_\odot$ model the overluminosity values are 0.15 and 0.25 dex, respectively. The extension of the loop for the 4 $M_\odot$ models is similar for the two He abundances, while for the 8 $M_\odot$ models the He-enhanced path is more extended in temperature of about 0.15 dex. The Padova tracks show a similar behaviour in luminosity, while the extension of the loop remains comparable for the two He values. In the Basti data base, there are not He-enhanced tracks for intermediate-mass stars in the He-burning evolutionary phase.

For what concerns differences in the stellar evolution codes and in the adopted input physics we focus on He-standard models (left-hand panel), because they are available in each data base (even with slightly different Y values), making possible a complete comparison. The left-hand panel of Fig. 2 shows that the tracks slightly differ in luminosity ($\Delta\log L/L_\odot \approx 0.1$ dex) and in the extension of the core-He burning loop ($\Delta\log T_{\rm eff} \lesssim 0.1$ dex). For example, the 4 $M_\odot$ ATON model (black line) is less luminous, but it has a blue loop more extended than the others. The behaviour in luminosity is the same for the model with 8 $M_\odot$, but in this case the Padova track extends to hotter temperatures. A deep analysis of the impact of different evolutionary codes and input physics on the evolutionary behaviour of stellar models is beyond the aim of this work, and we refer the interested reader to Chiosi & Matteucci (1982), Castellani, Chieffi & Straniero (1990), Ventura et al. (1998) and Ventura, Castellani & Straka (2005). The comparison illustrated above suggests that the number and the thermodynamic properties of the synthetic Cepheids may slightly change according to the used set of stellar models. However, the differences are expected to affect only marginally the main results obtained in this work. Consequently, the synthetic PLRs and PWRs based on evolutionary tracks by other authors show slopes and zero-points similar to ours, within the uncertainties. This is the case of results by Bono et al. (2010), whose relations are in very good agreement with ours, even taking into account that their Wesenheit relations are calculated by adopting $R_V = 3.23$ instead of $R_V = 3.1$. The PLRs and PWRs by Caputo, Marconi & Musella (2000) and Fiorentino et al. (2007) are also in agreement with our results, when statistical effects in the number of Cepheids are taken into account (see Table 7 in Section 4).

2 HE-ENHANCED CEPHEIDS AND COMPARISON WITH EMPIRICAL RELATIONS

Our models make possible to simulate the expected number and properties of Cepheids in stellar systems. In particular, we are interested to investigate the observational features of Cepheids in stellar

[1] http://pleiadi.pd.astro.it/
[2] http://basti.oa-teramo.inaf.it/

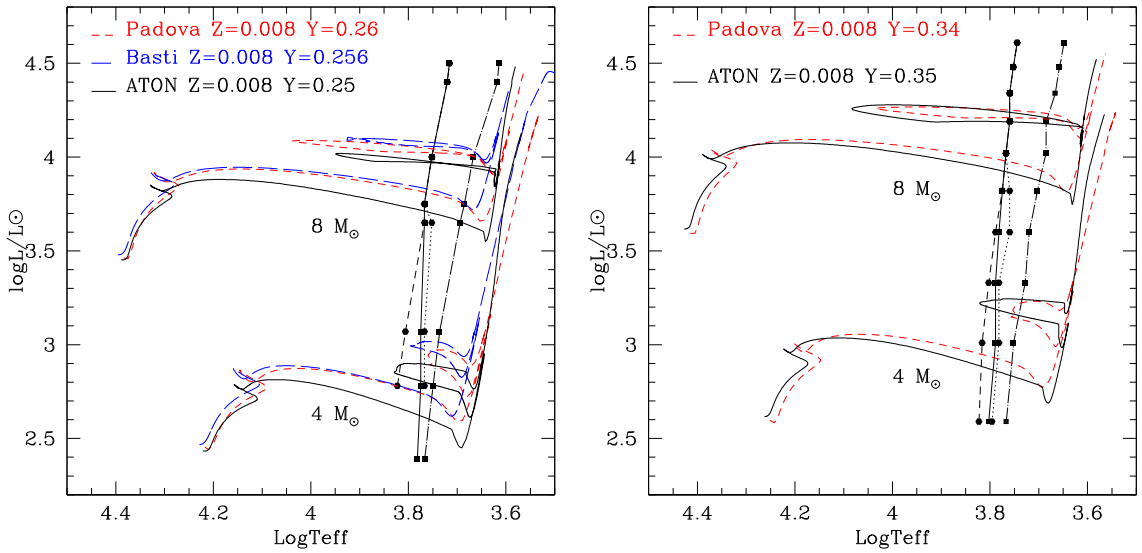

Figure 2. The evolutionary path in the HR diagram of a 4 $M_\odot$ and a 8 $M_\odot$ model calculated with the ATON code (black solid line) is compared to that from other data bases: Basti (long dashed blue line) and Padova (short dashed red lines) for $Y = 0.25$ (left-hand panel) and $Y = 0.35$ (right-hand panel, see the text). The FRE (dot dashed black line), FORE (dotted black line), FBE (solid black line) and FOBE (short dashed black line) derived in Carini et al. (2014) are also shown.

populations having a metallicity similar to the typical value of the LMC ($Z \sim 0.008$) and different He abundances: $Y = 0.25$, which represents the classical case, the higher value $Y = 0.35$, and a simple mixture of the two stellar populations. As a first step, we assembled together all the simulations computed assuming $Z = 0.008$ and $Y = 0.25$, considering all the ages. The resulting large sample of Cepheids corresponds to that of a stellar population generated from a series of close star-formation bursts with short age steps (2–10 Myr). It is worth noting that this can be considered as a stellar population whose stars are generated according to a constant star formation rate (SFR) from 20 to 250 Myr. We tested this assumption by computing a stellar population model in which a continue star formation is actually assumed in the same age interval. We found that the PLRs and the PWRs are in full agreement with those computed from the simulation described above, where the constant star formation has been reproduced by the series of SSPs with the adopted age steps. This is a well-known result in stellar population synthesis, as a complex stellar population can always be expanded in a series of SSPs (Renzini & Buzzoni 1986).

The same assembling procedure has been performed for $Y = 0.35$ models with age ranging from 20 to 150 Myr. We ended up with two stellar systems having a total mass in stars of $\sim 10^8 M_\odot$, and a total number of predicted Cepheids of $\sim$ 10 000 for $Y = 0.25$ and $\sim$ 7700 for $Y = 0.35$.

From the analysis of the two samples, we derived the PLRs and the PWRs in different photometric bands, namely in *B*, *V*, *I*, *J* and *K*, and *W*(*B*, *V*), *W*(*V*, *I*), *W*(*V*, *K*), *W*(*J*, *K*). The mean slopes and intercepts are reported in Table 3.

These theoretical relationships will be compared with the empirical ones, derived by observed samples of LMC Cepheids, in the following subsections.

2.1 PL relations

Our PLRs in the *V*, *I*, *J* and *K* bands are compared to those derived by Storm et al. (2011), who analysed 22 Cepheids pulsating in the fundamental mode in the LMC. The authors selected stars that simultaneously have high-quality near-infrared light curves from Persson et al. (2004) and very accurate optical photometry from OGLE-III (Soszynski et al. 2008; Udalski et al. 2008). Storm et al. (2011) determined the following relations from a linear regression to the absolute magnitudes and $\log P$, from the infrared surface brightness analysis:

$$M_V = -2.78\,(\log P - 1) - 4.00 \quad (1)$$

$$M_I = -3.02\,(\log P - 1) - 4.74 \quad (2)$$

$$M_J = -3.22\,(\log P - 1) - 5.17 \quad (3)$$

$$M_K = -3.28\,(\log P - 1) - 5.64. \quad (4)$$

Table 3. Theoretical PLRs and PWRs for fundamental classical Cepheids derived from a linear fit: M_λ (or $W_{\rm bands}$) $= \beta \times \log P + \alpha$. The standard deviation of the slopes σ_β and the intercepts σ_α are also reported.

Band	β	σ_β	α	σ_α
		$Z = 0.008$ $Y = 0.25$		
B	−2.598	0.006	−0.638	0.003
V	−2.836	0.005	−1.132	0.002
I	−3.003	0.003	−1.735	0.001
J	−3.137	0.003	−2.138	0.001
K	−3.252	0.002	−2.471	0.001
W(*B*,*V*)	−3.574	0.002	−2.664	0.001
W(*V*,*I*)	−3.262	0.002	−2.663	0.001
W(i)	−3.306	0.001	−2.645	0.001
W(*J*,*K*)	−3.318	0.001	−2.663	0.001
		$Z = 0.008$ $Y = 0.35$		
B	−2.591	0.015	−0.798	0.011
V	−2.859	0.011	−1.172	0.008
I	−3.053	0.008	−1.680	0.006
J	−3.195	0.006	−2.022	0.004
K	−3.319	0.004	−2.295	0.003
W(*B*,*V*)	−3.691	0.003	−2.332	0.002
W(*V*,*I*)	−3.350	0.003	−2.463	0.002
W(*V*,*K*)	−3.378	0.003	−2.441	0.002
W(*J*,*K*)	−3.390	0.003	−2.452	0.002

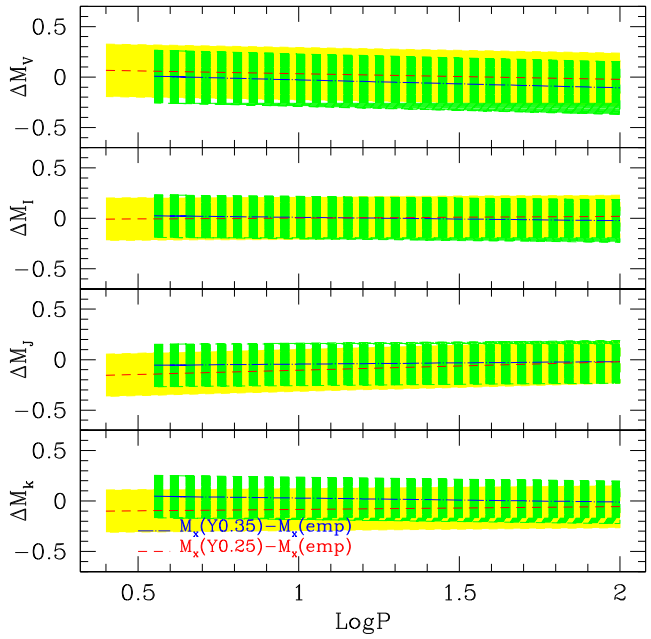

Figure 3. Differences between our theoretical and empirical PLRs in the *K*, *J*, *I* and *V* bands by Storm et al. (2011). The 1σ uncertainties are reported as filled yellow ($Y = 0.25$) and shaded green ($Y = 0.35$) areas.

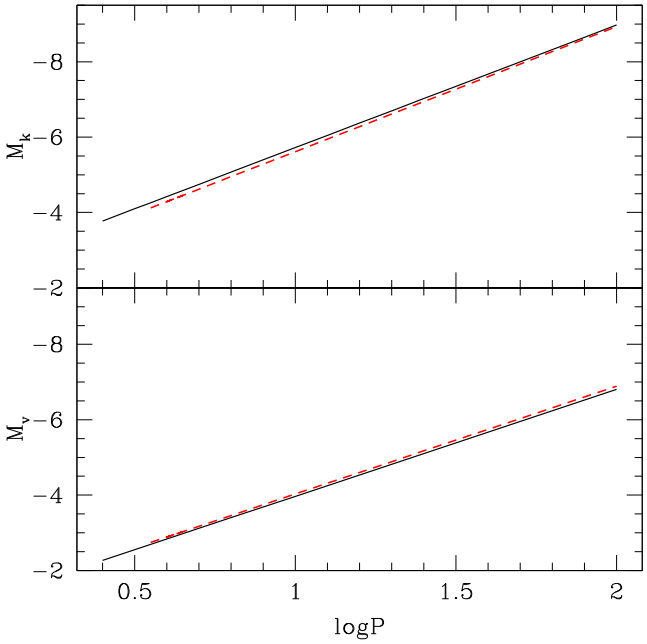

Figure 4. Comparison between the *V* (bottom panel) and *K* (top panel) relations with $Y = 0.25$ (black solid line), $Y = 0.35$ (red dashed line).

The dispersion around the fits is 0.26 mag in the *V* band and 0.21 mag in the others. Note that their relations are in good agreement with those of Persson et al. (2004) and Ripepi et al. (2012) in the near-infrared bands, and with Udalski (2000) and Soszynski et al. (2008) in the optical ones.

The relations above are in very good agreement within the uncertainties with our determinations (Table 3), as shown in Fig. 3, where the difference between the empirical and theoretical PLRs is reported as function of the photometric band.

The first thing that stands out is that the relations derived from models with the two considered *pure* He abundances are very similar. In each band, both the theoretical relations are in agreement with the empirical ones within the uncertainty, but a better agreement is found when assuming the standard He abundance. In the *K* band, the relation obtained from models with $Y = 0.35$ diverges from the observed ones at $\log P < 1.5$, with a maximum difference in magnitude of ∼0.05 mag at $\log P = 0.6$. The opposite trend is found in the *V* band, where the difference can be as high as 0.1 mag at $\log P > 1$, in agreement with the results of Fiorentino et al. (2002). The *I*- and *J*-band differences are negligible (≤0.1 mag). In conclusion, the uncertainties due to the helium abundance are of the order of 7 per cent in *B*, 4 per cent in *V*, 1 per cent in *I*, 1 per cent in *J* and 4 per cent in *K*.

The second thing that stands out is that the blue long dashed line, representing the difference between the theoretical relation with $Y = 0.35$ and the empirical one, moves from negative to positive values passing from the *V* to *K* band. This behaviour is more evident in Fig. 4, where the PLRs in *V* and *K* bands for both He abundances are compared.

The $\log P$–*V* relation with $Y = 0.35$ stands at brighter *V* magnitude for all periods, and the two lines are almost parallel each other. The $\log P$–*K* relations have the opposite behaviour and their magnitude difference decreases with the period. This happens because variable stars with the same period but different He abundance have very similar luminosity and surface gravity but different mass and effective temperature. In general, at fixed age, the He-rich stars are less massive (because their evolution is more rapid) but hotter than stars with standard He abundance. Since the bolometric correction in *V* (BC_V) decreases with effective temperature, while BC_K increases, it turns out that the behaviour in the $\log P$-mag relations is opposite. To clarify this point, we show in Table 4 the thermodynamic values, the magnitudes in the *V*, *I* and *K* bands and the bolometric corrections of two couple of variables with same period and age. We have chosen two stars at 130 and 30 Myr.

We can see the two stars in each couple mainly differ in mass and effective temperature. Higher is the temperature, higher is BC_K, but lower is BC_V; BC_I shows an intermediate behaviour. In the first case ($t = 130$ Myr), the temperature difference between the two stars is about 390 K; this implies a $\Delta BC_V = -0.07$ mag, $\Delta BC_I = 0.05$ mag, and $\Delta BC_K = 0.2$ mag. In the second case ($t = 30$ Myr), with a $\Delta T_{\rm eff} \sim 230$ K, the differences in the bolometric corrections are $\Delta BC_V = -0.09$ mag, $\Delta BC_I = 0.01$ mag and $\Delta BC_K = 0.12$ mag. Therefore, by increasing $\Delta T_{\rm eff}$, ΔBC_K increases, but ΔBC_V decreases. For this reason, the two relations $\log P$–*K* are inverted with respect to the $\log P$–*V* relations, and their magnitude difference is higher at shorter periods than at longer ones.

In conclusion, we confirm that the He content has an effect not detectable on the PLRs with the sensitivity of the current instruments, so that we cannot discriminate whether the population is He-enhanced or not. The $\log P$–*V* and $\log P$–*K* relations show an opposite behaviour that depends on the difference in the effective temperature between the variables having the same period but different He. This effect will be accentuated in the Wesenheit relations, which depends on the colour of the stars (see the next section).

2.2 Wesenheit relations

We compare our theoretical Wesenheit relations with the ones derived by Ripepi et al. (2012) and Inno et al. (2013). The former authors analysed K_s-band light curves of the Cepheids in the LMC

Table 4. Thermodynamic values, magnitudes in the V, I and K bands and the bolometric corrections of two couple of stars at $\log P = 0.6$ and 1.59, and age $t = 130$ and 30 Myr, respectively.

Y	t (Myr)	$M/M_\odot$	$T_{\rm eff}$ (K)	$\log(L/L_\odot)$	$\log g$	$\log P$	$V-K$ (mag)	V (mag)	I (mag)	K (mag)	BC_V (mag)	BC_I (mag)	BC_K (mag)
0.25	130	4.67	5495	3.06	1.97	0.60	1.65	−2.77	−3.50	−4.42	−0.13	0.60	1.51
0.35	130	3.84	5888	3.10	1.95	0.60	1.37	−2.94	−3.55	−4.31	−0.06	0.55	1.31
0.25	30	9.78	4897	4.19	0.93	1.59	2.22	−5.41	−6.37	−7.63	−0.32	0.64	1.90
0.35	30	7.82	5128	4.19	0.91	1.59	2.00	−5.50	−6.38	−7.50	−0.23	0.65	1.77

observed by the VISTA Magellanic Cloud survey[3] (VMC; Cioni et al. 2011; Ripepi et al. 2012). The stars are detected in the Y, J and K_s filters; the Cepheid K_s light curves are very well sampled, with at least 12 epochs and with typical errors of 0.01 mag. They mapped two fields centred on the south ecliptic pole and the 30 Doradus star-forming regions, respectively. We use only their results from the second field, because the sample is the richest one, being composed by 172 classical Cepheids pulsating in the fundamental mode and 150 in the first overtone. Since the longest period in the data set is 23 d, Ripepi and collaborators complemented the sample with literature data, including other 80 Cepheids pulsating in the fundamental mode from Persson et al. (2004). From all data, they derived

$$W(V, K) = -3.325 \log P + 15.870$$

with a dispersion of 0.078. No correction for the inclination of the LMC disc was applied.

We plot the comparison of the empirical relation with the present results in the top panel of Fig. 5. The theoretical relation obtained with the standard He abundance (red short-dashed line) overlaps the observed relation (black solid line) over the full range of periods, as clearly seen in the lower panel of the figure, where the difference between the empirical and theoretical PWRs is shown. The red line is nearly constant because the two relations are similar (throughout the paper, we assume the LMC distance modulus of $\mu = 18.50$), the small difference between the slopes of the two relations (0.019) leads to a maximum difference $\Delta W(V, K)$ of about 0.02 mag for $\log P > 1.8$. Instead, the PWR derived from He-enhanced models (blue dot–long-dashed line) is tilted with respect to the observational one: the difference between the slopes is large reaching nearly 0.15 mag at short periods ($\log P \sim 0.6$), because the He-enhanced models predict fainter magnitudes for the periods considered in this work. As we have already mentioned, the shortest period reached is $\log P \sim 0.5$, because in stellar populations older than about 150 Myr stars do not cross the instability strip during their evolution; therefore, there are not Cepheids with $Z = 0.008$, $Y = 0.35$ and $\log P < 0.5$.

To investigate this issue in other photometric bands, we consider the PWRs published by Inno et al. (2013). They combined the data in the V and I bands of the OGLE III (Optical Gravitational Experiment) catalogue[4] (Soszynski et al. 2008) with data in the J, H and K bands from the near-infrared catalogue of IRSF/SIRIUS Near-Infrared Magellanic Clouds Survey provided by Kato et al. (2007), ending up with a sample of 1840 fundamental classical-Cepheids in the LMC. From linear regressions, the authors found

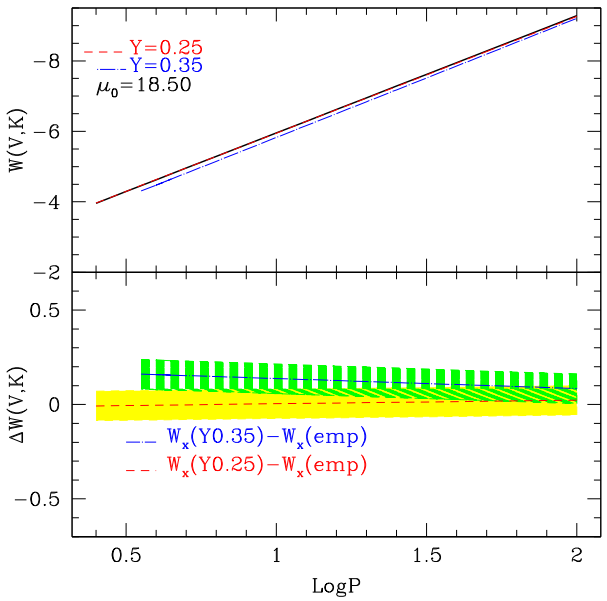

Figure 5. Upper panel: comparison between the $W(V, K)$ relation (black solid line) of Ripepi et al. (2012) and the theoretical ones: the red short-dashed line corresponds to $Y = 0.25$ and the blue dot–long dashed line to $Y = 0.35$ (see Table 3). Lower panel: difference between theoretical and empirical Wesenheit relations plotted in the upper panel. The used distance modulus of the LMC is 18.50 mag (Ripepi et al. 2012). Symbols and colours are as in the previous figure.

$$W(V, K) = -3.326 \log P + 15.901 \quad (5)$$

$$W(V, I) = -3.327 \log P + 15.899 \quad (6)$$

$$W(J, K) = -3.365 \log P + 15.876. \quad (7)$$

The dispersion obtained is 0.07 mag for $W(V, K)$ and $W(V, I)$, and 0.08 mag for $W(J, K)$.

Again, the good agreement between our theoretical standard He-abundance and the observational Wesenheit relations is evident in Fig. 6. Small differences arise in the zero-points and the slopes, up to ∼− 0.03 mag for $W(V, K)$ (lower panel), while from nearly −0.02 to 0.06 mag for $W(J, K)$ (middle panel) and from nearly −0.04 to 0.08 mag for $W(V, I)$ (top panel); that is, our standard relations are in agreement with the empirical ones within the errors over the full range of periods. In the case of $Y = 0.35$, the relations are tilted with respect to the observational ones, the difference reaching values larger than ∼0.15 mag. This result implies that, if all stars in a generic stellar population have an enhanced He abundance, the uncertainty in the evaluation of the distance will be as high as 0.1–0.15 mag. To enlighten this point, let us suppose that one is observing a sample of Cepheids all having an He abundance

[3] Based on observations made with ESO Telescopes at the La Silla or Paranal Observatories under programme ID(s) 179.B-2003(D), 179.B-2003(C), 179.B-2003(B).
[4] http://ogledb.astrouw.edu.pl/∼ogle/CVS/

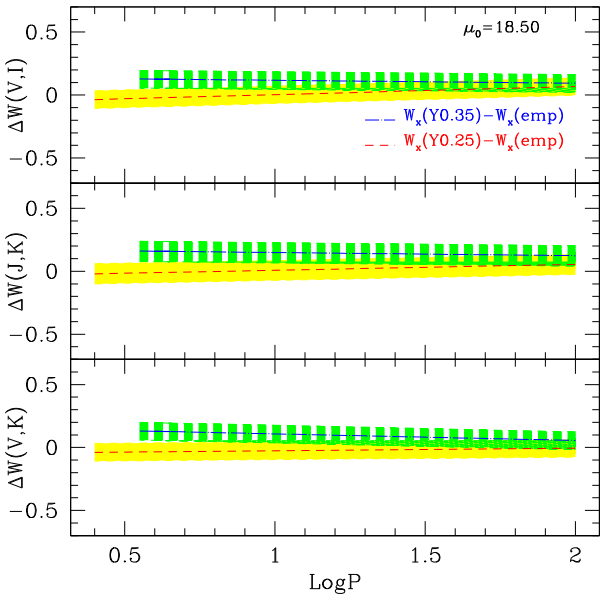

Figure 6. Difference between theoretical and empirical PWRs by Inno et al. (2013) in the (V, I), $W(J, K)$ and (V, K) bands. Symbols and colours are as in the previous figure.

$Y \sim 0.35$. If the He-standard Wesenheit relations are used, it leads to a systematic error of the order of 3–7 per cent in evaluating the distance modulus, with the error increasing when $\log P$ decreases. For example, in the case of $W(V,I)$, the systematic error is about 3 per cent.

2.3 Mixed population

Before concluding the section, we perform a numerical exercise to study the case where the two populations are mixed together. Since our models foresee 9918 Cepheids for $Y = 0.25$ and 7641 for $Y = 0.35$, the contamination of He-enhanced stars is of the order of 40 per cent. We test this population split, because it can be considered one of the worst case scenarios, useful to derive an upper limit of the uncertainty on the galaxy distances caused by different helium abundances in the galaxy field populations. In addition, it may be interesting for young cluster populations.

In this case, the relations are tilted with respect to those with a *pure* abundance of He, as already shown in Carini et al. (2014). Here, we extended the computation and the results on PLRs and PWRs as reported in Table 5. The systematic uncertainty in the evaluation of distances can be considered negligible only in the I band, because the PLR of the mixed population is similar (within ∼1 per cent) to the one derived for a *pure* $Y = 0.25$ population. The other uncertainties are 12 per cent, 5 per cent, 5 per cent, and 10 per cent for the B, V J and K bands and decrease when the period decreases. Since the PLR in the K band is less affected by systematic errors due, for example, to the finite width of the instability strip, non-linearity and chemical composition (e.g. Bono et al. 1999b; Caputo et al. 2000) or reddening and intrinsic dispersion (e.g. Madore & Freedman 1991) and to stochastic effects (see Table 7 in Section 4), the effect of helium seems to be the potentially the most important one. This becomes particularly evident in the case of mixed population, where the uncertainty due to the helium effect on the distance determination can be as high as 10 per cent. This can be seen in the upper panel of Fig. 7, that shows, the PLRs in the K band for three different cases: *pure* $Y = 0.25$ (black solid line), *pure* $Y = 0.35$ (red dotted line) and the mixed population $Y_{\rm MIXED}$ (blue dot–long dashed line). The black solid line and the red dotted line are nearly superimposed, while the third line is tilted with respect to the other ones, particularly for $\log P > 1.0$. This is more evident in the bottom panel of the same figure, where the difference between the empirical M_k relation by Storm et al. (2011) and our theoretical relation obtained from a *pure* $Y = 0.25$ (red short-dashed line) and from the mixed population (blue dot–long dashed line) are shown.

Table 5. Theoretical PLRs and PWRs for fundamental classical Cepheids derived from a linear fit for a mixed population containing stars with $Y = 0.25$ and $Y = 0.35$ ($Y_{\rm MIXED}$): M_λ [or $W(\text{band}_1, \text{band}_2)$] $= \beta \times \log P + \alpha$. The standard deviation of the slopes σ_β and the intercepts σ_α are also reported.

Band	β	σ_β	α	σ_α
		$Z = 0.008$ $Y_{\rm MIXED}$		
B	−2.784	0.005	−0.612	0.003
V	−2.909	0.004	−1.120	0.002
I	−2.989	0.003	−1.733	0.002
J	−3.057	0.002	−2.146	0.001
K	−3.109	0.002	−2.487	0.001
$W(B,V)$	−3.296	0.003	−2.695	0.002
$W(V,I)$	−3.113	0.002	−2.678	0.001
$W(V,K)$	−3.135	0.002	−2.664	0.001
$W(J,K)$	−3.139	0.002	−2.683	0.001

The PWRs show the same behaviour (Fig. 7, right-hand panel); the empirical $W(V, K)$ relation is by Ripepi et al. (2012). The error in the distance determinations from the PWRs could be as high as 10 per cent (or more) for $\log P > 1.5$. At shorter periods the error decreases, for example at $\log P = 1$, it is about 7 per cent. These percentages are similar in the different bands.

The unexpected behaviour in the case of the mixed population is due to the different distribution of Cepheids. In fact, by modelling the distributions one finds:

– at $\log P < 0.5$Cepheids with $Y = 0.25$ are brighter and more numerous than ones with $Y = 0.35$:
$N_{Y=0.25}(\log P < 0.5) = 8503$,
$N_{Y=0.35}(\log P < 0.5) = 0$;
– for $0.5 \leq \log P \leq 1$the Cepheids with $Y = 0.25$ are brighter and less numerous than the ones with $Y = 0.35$ ($\Delta W(V, K)$) ∼ 0.15 mag):
$N_{Y=0.25}(0.5 \leq \log P \leq 1.0) = 1193$,
$N_{Y=0.35}(0.5 \leq \log P \leq 1.0) = 7171$;
– for $1.0 < \log P \leq 1.5$the number of stars for both $Y = 0.25$ and $Y = 0.35$ are much less numerous than that found at shorter periods:
$N_{Y=0.25}(1.0 < \log P \leq 1.5) = 144$,
$N_{Y=0.35}(1.0 < \log P \leq 1.5) = 409$;
– for $1.5 < \log P \leq 2.0$the number of Cepheids are much less numerous than ones found at shorter periods:
$N_{Y=0.25}(1.5 < \log P \leq 2.0) = 76$,
$N_{Y=0.35}(1.5 < \log P \leq 2.0) = 59$.

The distributions described above show that the mixed population considered here is composed of two major bulks of Cepheids, one at $\log P < 0.5$ ($Y = 0.25$) and the second one at $0.5 < \log P < 1.0$ ($Y = 0.35$), with the latter fainter than typical Cepheids with $Y = 0.25$. This forces a simple linear fitting to provide a relation more tilted than that from a *pure* He abundance population.

In other words, at $\log P \lesssim 1$ a sample fully composed by Cepheids with a standard and a sample with enhanced He content produce very similar PWRs. Therefore, if the samples used to calibrate the relations contain, in addition to Cepheids with standard He

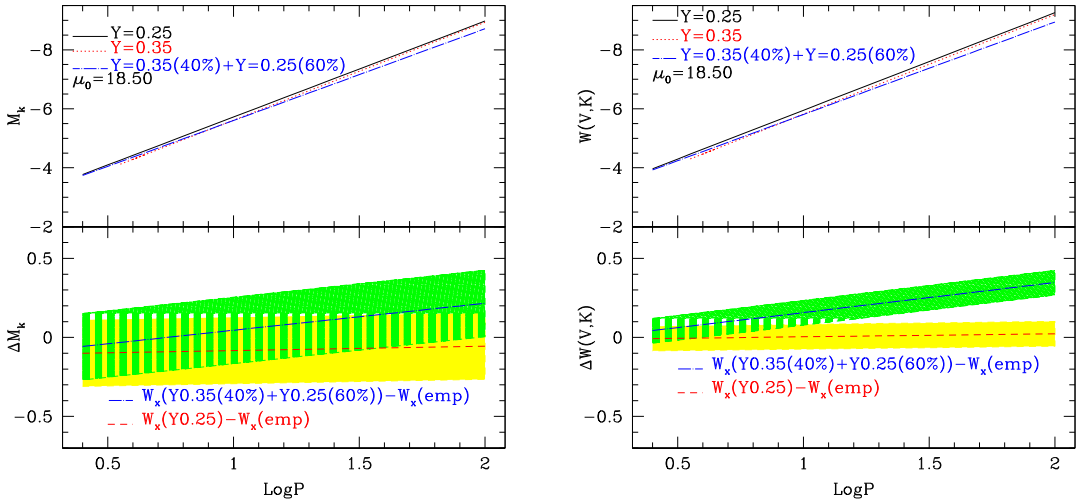

Figure 7. Upper panels: comparison between the $P - M_k$ (left-hand panel) and $W(V, K)$ (right-hand panel) relations derived from a pure $Y = 0.25$ population (black solid line), pure $Y = 0.35$ population (red dotted line), and a mixed population $Y_{\rm MIXED}$ [60 per cent (0.25); 40 per cent (0.35)] (blue dot–long dashed line). Lower panel: the differences between theoretical and empirical relations, i.e. $M_k[Y = 0.25] - M_k$[empirical] (right-hand panel), $W(V, K)[Y = 0.25] - W(V, K)$[empirical] (left-hand panel) represented by a red short-dashed line, and $M_k[Y_{\rm MIXED}$[60 per cent(0.25); 40 per cent(0.35)]] $- M_k$[empirical] (right-hand panel) and $W(V, K)[Y_{\rm MIXED}$[60 per cent(0.25); 40 per cent(0.35)]] $- W(V, K)$[empirical] (left-hand panel) represented by a blue dot–long-dashed line. The empirical $P - M_k$ relation is from (Storm et al. 2011 ($P - M_k$), while the $W(V, K)$ relation is from Ripepi et al. 2012). The 1σ uncertainties are reported as filled yellow ($Y = 0.25$) and shaded green ($Y_{\rm MIXED}$[60 per cent(0.25); 40 per cent(0.35)]).

abundances ($Y = 0.24 - 0.25$), variables with a He abundance up to 0.35, these latter stars do not affect the calibration relations significantly. A different behaviour is expected at longer periods, where a high contamination of He-enhanced Cepheids (>40 per cent) may affect the derived relationships. Of course, these results require further work with different mixture of stellar populations. Nevertheless, it provides interesting warning against simple interpolation between pure populations to infer indications on properties of mixed population.

3 COMPARISON WITH CEPHEIDS IN LMC

We used our models to search for systematic effects possibly associated with the presence of Cepheids with higher He abundances with respect to the primordial value in an observed sample. As a true observational sample, we adopt the Cepheids of the OGLE III catalogue (Soszynski et al. 2008) for the data in the *V* and *I* band, and the VMC (Cioni et al. 2011; Ripepi et al. 2012) for the *Ks* magnitudes. The first catalogue includes 3361 classical Cepheids, 1848 of them pulse in the fundamental mode. The stars are detected in the *V* and *I* bands, the accuracy of the photometric calibrations is better than 0.02 mag. Since the Cepheids are distributed along all the LMC, a differential reddening is expected (e.g. Zaritsky, Gonzalez & Zabludoff 2004; Soszynski et al. 2008). The presence of a differential reddening affecting the LMC Cepheids in the OGLE sample broadens the observed sequences (see below) and the uncertainty on the apparent magnitude increases. For example, we estimated from Fig. 8 a spread of the order of 0.2 mag at $\log P = 0.6$. The second catalogue is described in Section 2.2.

In Fig. 8, observational data (red circles) are compared with Cepheids predicted by models described in Section 1.2 with both He abundances ($Y = 0.25$, blue triangles; $Y = 0.35$, green squares), in the *V* (left-hand panel), *I* (central panel) and K_s (right-hand panel) bands.

We note that a detailed simulation of LMC SFR in beyond the aim of this paper. Differently from what assumed in our models, where a constant SFR in the age interval 20–250 Myr is adopted, recent LMC SFR estimations are found to vary greatly from subregion to subregion (e.g. Rubele et al. 2012, and reference therein); hence, we prefer to not introduce a further not well-known parameter in the present discussion. The predicted variables occupy the same region of the diagram independently of the He content, and all of them overlay the observed ones; therefore, the presence of He-enhanced stars in the observed sample is not to be excluded. From the comparison, it is clear that in the period range typical of LMC Cepheids, it is difficult to disentangle the two He abundances. We stress that the comparison is only a by-eye analysis (including projection effect and differential reddening effects), while the coefficients of the PLRs and of the PWRs offer a more robust test for disentangling the two populations. From them, it appears that the use of a He-enhanced population gives discrepancies with what is observed, supporting the lack of an He-rich population in the LMC, together with different initial condition in the formation of the explored LMC regions and GCs, as well as it was found for open clusters (Bragaglia et al. 2014).

To investigate in more details the possible presence of He-enhanced Cepheids, we need to study simultaneously the period, the age and the magnitude of variables. This is because He-enhanced stars evolve more rapidly, they are brighter and pulsate with a longer period with respect to Cepheids of same mass but with $Y = 0.25$. Note that, as we have already shown, Cepheids with $\log P \lesssim 0.5$ cannot be He-enhanced stars.

Our models also predict a non-negligible number of Cepheids (∼200 for $Y = 0.25$ and 60 for $Y = 0.35$) at $\log P > 1.5$ and many (hundreds) with $\log P < 0.4$ not present in the OGLE III catalogue. The long-period Cepheids are very bright ($M_I \lesssim -6.0$ mag) and have an age $t \lesssim 40$ Myr, the short periods ones have $M_I < -2.0$ mag and $t > 150$ Myr. The lack of Cepheids observed at $\log P > 1.5$ could be due to several reasons including a bias effect in the observations. In the OGLE III catalogue, the most bright stars ($I > 13$ mag) are saturated in the *I* band and they are not measured in the *V* filter, for the latter filter the saturation starts to be relevant at periods longer

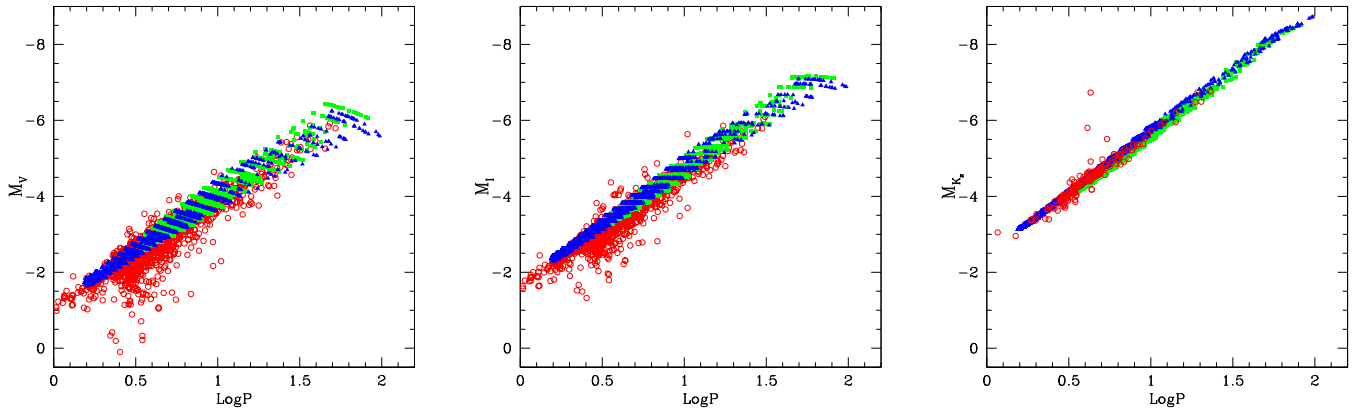

Figure 8. Period–luminosity diagram in the V and I and K_s bands for the classical fundamental-mode Cepheids in the LMC, taken from the catalogue OGLEIII (V and I) and VMC (K_s) (red circles). The blue triangles and green squares are the simulation done with $Y = 0.25$ and $Y = 0.35$, respectively.

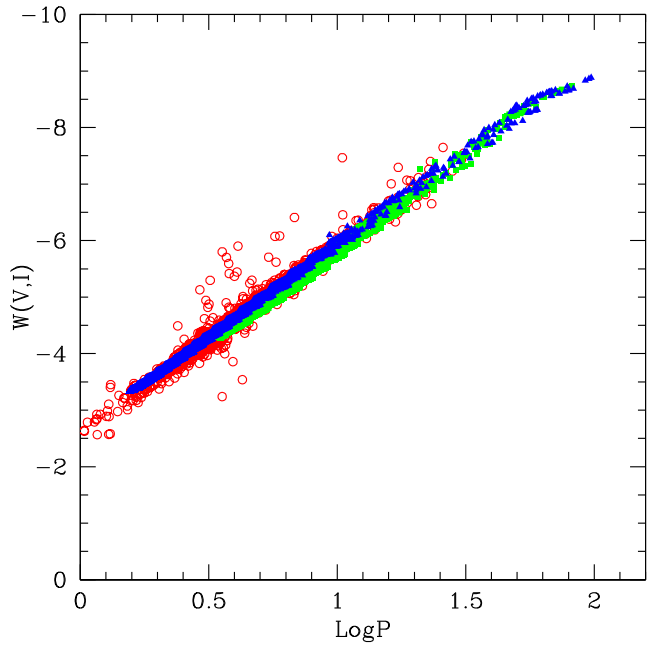

Figure 9. Period–W(V,I) diagram for the classical fundamental-mode Cepheids in the LMC, taken from the catalogue OGLEIII (red circles). Symbols are the same as in the previous figures.

than ∼50 d (Fig. 8, right-hand panel). Moreover, in the OGLE III catalogue the Cepheids with $\log P < 0.4$ suffer of incompleteness because in this domain the PL sequences overlap with various types of pulsating variables, so it is difficult to distinguish the characteristic shapes of the light curves of Cepheids. In the VMC catalogue, the magnitude limits in the K_s band of the Cepheids sample are $11.4 \lesssim K_s \lesssim 20.7$ mag.

From the figure, we also note a large dispersion in magnitude in the V and I bands, which is due to differential reddening as we have already mentioned. This is also supported by the small dispersion found in the K_s band (see the left-hand panel of Fig. 8). Further, if we use the Wesenheit relations this spread disappears, as shown in Fig. 9 (the symbols are the same of Fig. 8). Again, simulated Cepheids with both the He abundances overlap very well the observational data.

4 STOCHASTIC EFFECTS DUE TO THE NUMBER OF CEPHEIDS

In this section, we analyse how the number of Cepheids included in the sample affects the determination of the slope and zero-point of PL and PW relationships, that is the distance evaluation. To this purpose, by taking advantage of the Monte Carlo procedures used to simulate stellar populations, we used the results obtained from our sets of models. We assembled together the Cepheids belonging to each simulation at different ages and fixed chemical composition, ending up with 100 independent samples of Cepheids. Each sample contains nearly 50–100 Cepheids. Hereinafter, we refer to these small samples of Cepheids as mini-samples.

The standard procedure to derive distance moduli is to determine the magnitude difference between the individual star and the adopted reference relation and then average these values. Following this procedure for each mini-sample, we quantify the stochastic uncertainties due to the small number of Cepheids of a given stellar population. To this aim, we computed the difference between the magnitude of the Cepheids of each mini-sample with the one obtained using the reference PL relations for each photometric band (Table 3). For each mini-sample, the average of these differences is obviously equal to zero ($\sim 10^{-4}$) because we are dealing with absolute magnitudes. What is interesting is the standard deviation (σ) that provides the theoretical evaluation of the stochastic uncertainty. This is shown in Fig. 10, where the σ values in the V and K bands are plotted for all our mini-samples and for the two helium abundances. The average values are marked as red lines and reported in Table 6. The uncertainties decrease from optical to near-infrared bands for both He abundances: for Cepheids with $Y = 0.25$ in the B and V bands the σ is as high as 0.14 and 0.10 mag, respectively, while in the K band it reaches 0.04 mag. This implies that, infrared measurements remain quite reliable for deriving the galaxy distances even taking into account the stochasticity. As far as the He abundance is concerned, the stochastic uncertainties for $Y = 0.35$ appear slightly more relevant than for $Y = 0.25$.

The procedure described above has been adopted to evaluate the stochastic uncertainties to derive distances with the Wesenheit relations and, the results are presented in Table 6. Once again, the powerfulness of the Wesenheit relations is confirmed; in fact, the values of the distance uncertainties are nearly one order of magnitude smaller than what found for PLRs. In particular, the 1σ is of the order of 0.03 for $Y = 0.25$ and ~ 0.04 for $Y = 0.35$. This can be seen in the lower panels of Fig. 10.

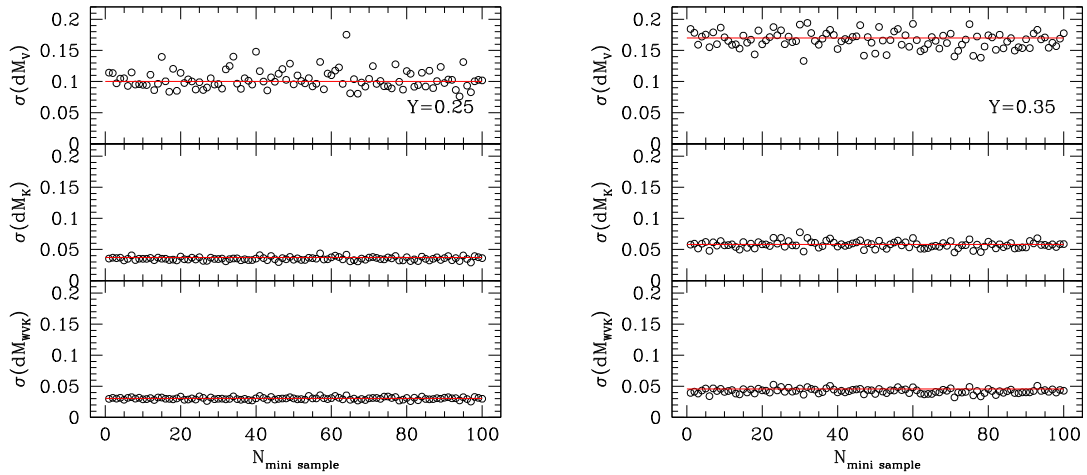

Figure 10. Standard deviations of the differences between the magnitude calculated with the reference relation and that derived from evolution models. This procedure is done for each mini-sample in the V band (top panels) and K band (middle panels), and for $W(V, K)$ in the lower panels. The red horizontal lines are the mean values of standard deviations. Results for $Y = 0.25$ ($Y = 0.35$) are reported in the left-hand (right-hand) panels.

Table 6. Mean standard deviations of the differences between the simulated magnitude of stars in each mini-sample and that calculated from the reference relations, representing the distance modulus dM_X, where X refers to the generic band.

Y	$\sigma(dM_B)$ (mag)	$\sigma(dM_V)$ (mag)	$\sigma(dM_I)$ (mag)	$\sigma(dM_J)$ (mag)	$\sigma(dM_K)$ (mag)	$\sigma(dM_{W(B,V)})$ (mag)	$\sigma(dM_{W(V,I)})$ (mag)	$\sigma(dM_{W(V,K)})$ (mag)	$\sigma(dM_{W(J,K)})$
0.25	0.14	0.10	0.07	0.05	0.04	0.04	0.04	0.03	0.03
0.35	0.22	0.17	0.12	0.09	0.06	0.04	0.05	0.05	0.04

Table 7. Mean, minimum and maximum values of the slopes and intercepts of the log P–mag and log P–W relations with the respective errors ($X = a \log P + b$).

Band	$a_{\rm mean}$	σ_a	$b_{\rm mean}$	σ_b	$a_{\rm min}$	$b_{\rm min}$	$a_{\rm max}$	$b_{\rm max}$
				$Z = 0.008$ $Y = 0.25$				
B	−2.634	0.177	−0.626	0.053	−3.040	−0.518	−2.217	−0.759
V	−2.859	0.125	−1.125	0.037	−3.141	−1.050	−2.570	−1.217
I	−3.018	0.088	−1.730	0.026	−3.210	−1.679	−2.815	−1.787
J	−3.144	0.057	−2.136	0.017	−3.267	−2.104	−3.000	−2.176
K	−3.252	0.032	−2.471	0.010	−3.320	−2.450	−3.161	−2.495
W(B,V)	−3.556	0.058	−2.670	0.018	−3.662	−2.635	−3.436	−2.705
W(V,I)	−3.262	0.036	−2.662	0.011	−3.333	−2.641	−3.163	−2.689
W(V,K)	−3.303	0.025	−2.646	0.008	−3.351	−2.632	−3.235	−2.663
W(J,K)	−3.314	0.023	−2.664	0.007	−3.357	−2.651	−3.249	−2.682
				$Z = 0.008$ $Y = 0.35$				
B	−2.591	0.183	−0.799	0.123	−3.149	−0.441	−2.225	−1.016
V	−2.857	0.134	−1.174	0.090	−3.266	−0.911	−2.591	−1.326
I	−3.049	0.098	−1.682	0.066	−3.347	−1.490	−2.854	−1.796
J	−3.191	0.073	−2.025	0.049	−3.410	−1.882	−3.049	−2.107
K	−3.314	0.051	−2.298	0.034	−3.458	−2.203	−3.204	−2.361
W(B,V)	−3.680	0.052	−2.339	0.035	−3.807	−2.261	−3.534	−2.428
W(V,I)	−3.346	0.049	−2.466	0.033	−3.472	−2.382	−3.236	−2.531
W(V,K)	−3.374	0.043	−2.444	0.029	−3.491	−2.357	−3.268	−2.521
W(J,K)	−3.386	0.041	−2.455	0.028	−3.507	−2.366	−3.279	−2.532

Following a different approach, the slopes of the PL and PW relations for each mini-sample (containing 50–100 Cepheids) are also computed. Clearly, they change respect to the reference ones reported in Table 3, due to the smaller number of Cepheids. Table 7 lists the mean, minimum and maximum, values of the slopes and the intercepts for all the computed log P–L and log P–W relations and their standard deviation. As expected, the mean values converge to the ones derived in the previous section from a larger sample of Cepheids (see Table 3), but here, the dispersions are larger.

Recalling that our mini-samples collect $\sim$ 50 Cepheids, this exercise evaluates the reliability of PLRs and PWRs when they are derived from small samples of variables. As a result, we find that samples containing few tens of Cepheids could be not adequate to derive the PLRs and PWRs. In fact, as representative of worst cases, the minimum and maximum slopes differ significantly. For instance, the slope of the $\log P$–M_I relation changes from -3.2 to -2.8 for $Y = 0.25$ and from -3.3 to -2.9 when $Y = 0.35$. Note that the present results are consistent with the analysis presented in Carini et al. (2014, see table 5). Therefore, as anticipated in Section 2.3, the K band minimizes the impact of the statistics, both in the PLR and PWR. Variations of the He abundance do not change this behaviour. One should keep in mind that the magnitude differences we have analysed can be interpreted as the 1σ uncertainties due to statistical effects that we have when the distance modulus of a galaxy is derived by using a PLR obtained from a poor sample of Cepheid stars.

5 SUMMARY AND CONCLUSIONS

We simulated the observational properties of Cepheids belonging to stellar populations with metallicity $Z = 0.008$ and two different He abundances, $Y = 0.25$ and $Y = 0.35$, in the age interval 20–250 Myr ($Y = 0.25$) and 20–150 Myr ($Y = 0.35$). With the help of population synthesis models we investigated and quantified if and how the presence of He-enhanced Cepheids in the observed samples could contribute to the PLRs and PWRs and to their uncertainty.

We find that Cepheids pulsating in the fundamental mode belonging to a stellar population with $Y = 0.35$ and $\log P \lesssim 0.5$ or with $Y = 0.25$ and $\log P \lesssim 0.2$ should not be observed, because these stars, during the He-burning phase, do not cross the instability strip. We analysed our whole sample of synthetic Cepheids and derived the PLRs and PWRs in different photometric bands from the optical to near-infrared wavelengths. The comparison between our theoretical and empirical relationships, obtained by Storm et al. (2011), Ripepi et al. (2012) and Inno et al. (2013) from multiwavelength data sets of LMC, discloses a very good agreement in the case of synthetic Cepheids with an He abundance $Y = 0.25$, metallicity $Z = 0.008$ and Salpeter IMF.

We find that the differences in the PLRs obtained from stellar populations having different He abundance has a negligible impact (few percents) on the distance determination. Instead, if a mixed population of Cepheids (composed by $\sim$ 60 per cent of variables with $Y = 0.25$ and $\sim$40 per cent with $Y = 0.35$) is present in the observed sample and compared to empirical PLRs and PWRs to derive distances, the possible systematic uncertainties can be of the order of $\sim$5–10 per cent at $\log P > 1.5$, while at shorter periods the error is less than 7 per cent, independently from the band taken into account. In the I band the uncertainty is of the order of 1 per cent independently from the period. In addition, in the case of $Y = 0.35$, the Wesenheit relations are slightly tilted with respect to the empirical ones. Therefore, in principle, when evaluating the distance of a generic stellar population containing He-enhanced stars with the quoted metallicity, the uncertainty due to the helium abundance could be not negligible, being the systematic error of the order of 5–10 per cent in all bands for $\log P < 1$, with the exception of the $W(V, I)$ for which the error is as small as $\sim$3 per cent.

With the aim of investigating the presence of He-enhanced Cepheids in an observed sample of variables, we compared our simulations with Cepheids in the LMC listed in the OGLE III and the VMC catalogues, finding a very good agreement. Unfortunately, there is not a clear separation between Cepheids having different He abundances, and some refinements in understanding Cepheids in LMC are still needed.

Finally, we studied the uncertainty introduced in the distance estimations when one deals with a small number of Cepheids (few tens) and derived the corresponding PL and PW relations.

Our analysis shows that the stochastic uncertainties due to the small number of Cepheids ($\sim$ 50) used to derive distances with the Wesenheit procedure is nearly negligible ($1\sigma \lesssim 0.04$ mag) in all bands and for both He values investigated here. Larger uncertainties are found for PL relations. Nevertheless, the 1σ uncertainties in the B band is ~ 0.14 mag for $Y = 0.25$, while it becomes much smaller for the K band ($\sim$0.04 mag). As far as it concerns $Y = 0.35$, the uncertainties are slightly larger, ranging from ~ 0.22 mag for the B band up to 0.06 for the K band. From the present analyses we conclude that, in the optical bands, the population stochastic effect appears to be larger than the He effect on the estimation of the PLRs and PWRs, hence on the evaluation of the cosmological distance. We showed that the stochastic uncertainties are minimized in the NIR bands.

In conclusion, this study suggests that when information on the He abundance of the Cepheids in a galaxy are not available and the variables are compared to PLRs and PWRs obtained from local samples, the derived distances might be affected by non-negligible systematic uncertainties of the order of a few percent. These uncertainties are more effective if the number of Cepheids observed in the given galaxy is small. The effect appears more severe for optical than for near-infrared bands. Nevertheless, we found that PLR in the K band ($\log P \lesssim 1.5$) seems to be the relation most affected by variations in the helium content. These results for the K band are particularly interesting in view of future Cepheid observations with the James Webb Space Telescope. Further fundamental step on this issue will also be provided by the large sample of Cepheids properties expected from the *Gaia* mission (Clementini et al. 2016) and in the faraway future from the LSST survey.

ACKNOWLEDGEMENTS

It is a pleasure to thank the referee for her/his useful suggestions and comments. This work received partial financial support by INAF−PRIN2014 '*EXCALIBURS: EXtragalactic distance scale CALIBration Using first – Rank Standard candles*' (PI G. Clementini).

REFERENCES

Bastian N., Lamers H. J. G. L. M., de Mink S. E., Longmore S. N., Goodwin S. P., Gieles M., 2013, MNRAS, 436, 2398
Bertelli G., Nasi E., Girardi L., Marigo P., 2009, A&A, 508, 355
Blöcker T., 1995, A&A, 297, 727
Bono G., Caputo F., Marconi M., 1998, ApJ, 497, L43
Bono G., Marconi M., Stellingwerf R., 1999a, ApJS, 122, 167
Bono G., Caputo F., Castellani V., Marconi M., 1999b, ApJ, 512, 711
Bono G., Caputo F., Cassisi S., Marconi M., Piersanti L., Tornambè A., 2000, ApJ, 543, 955
Bono G., Gieren W. P., Marconi M., Fouqué P., Caputo F., 2001, ApJ, 563, 319
Bono G., Caputo F., Marconi M., Musella I., 2010, ApJ, 715, 277
Bragaglia A., Sneden C., Carretta E., Gratton R. G., Lucatello S., Bernath P. F., Brooke J. S. A., Ram R. S., 2014, ApJ, 796, 68
Brocato E., Castellani V., Raimondo G., Romaniello M., 1999, A&AS, 136, 65
Brocato E., Castellani V., Poli F. M., Raimondo G., 2000, A&AS, 146, 91
Canuto V., Mazzitelli I., 1991, ApJ, 370, 295

Caputo F., Marconi M., Musella I., 2000, A&A, 354, 610
Carini R., Brocato E., Marconi M., Raimondo G., 2014, A&A, 561, A110
Carretta E. et al., 2009a, A&A, 505, 117
Carretta E., Bragaglia A., Gratton R., D'Orazi V., Lucatello S., 2009b, A&A, 508, 695
Castellani V., Chieffi A., Straniero O., 1990, ApJS, 74, 463
Castelli F., Kurucz R. L., 2003, in Piskunov N., Weiss W. W., Gray D. F., eds, Proc. IAU Symp. Vol. 210, Modelling of Stellar Atmospheres. Kluwer, Dordrecht, p. 20
Chiosi C., Matteucci F. M., 1982, A&A, 105, 140
Cioni M.-R. L. et al., 2011, A&A, 527, A116
Clementini G. et al., 2016, A&A, 595, A133
Cloutman L. D., Eoll J. G., 1976, ApJ, 206, 548
D'Ercole A., Vesperini E., D'Antona F., McMillan S., Recchi S., 2008, MNRAS, 391, 825
De Marchi G. et al., 2016, MNRAS, 455, 4373
de Mink S. E., Pols O. R., Langer N., Izzard R. G., 2009, A&A, 507, L1
Decressin T., Charbonnel C., Meynet G., 2007, A&A, 475, 859
Efstathiou G., 2014, MNRAS, 440, 1138
Fiorentino G., Caputo F., Marconi M., Musella I., 2002, ApJ, 576, 402
Fiorentino G., Marconi M., Musella I., Caputo F., 2007, A&A, 476, 863
Fouqué P. et al., 2007, A&A, 476, 73
Freedman W. L., Madore B. F., 2010, ApJ, 719, 335
Freedman W. L. et al., 2001, ApJ, 553, 47
Gratton R., Sneden C., Carretta E., 2004, ARA&A, 42, 385
Gratton R. G., Carretta E., Bragaglia A., Lucatello S., D'Orazi V., 2010, A&A, 517, A81
Gratton R. G., Carretta E., Bragaglia A., 2012, A&AR, 20, 50G
Grevesse N., Sauval A., 1998, Space Sci. Rev., 85, 161
Inno L. et al., 2013, ApJ, 764, 84
Kato D. et al., 2007, PASJ, 59, 615
Kennicutt R. C., Jr, et al., 1998, ApJ, 498, 181
Madore B. F., 1982, ApJ, 253, 575
Madore B., Freedman W., 1991, PASP, 103, 933
Marconi M., Musella I., Fiorentino G., 2005, ApJ, 632, 590
Marconi M. et al., 2010, ApJ, 713, 615
Marino A. F. et al., 2014, MNRAS, 437, 1609
Milone A. P., Bedin L. R., Piotto G., Anderson J., 2009, A&A, 497, 755
Milone A. P., Marino A. F., D'Antona F., Bedin L. R., Da Costa G. S., Jerjen H., Mackey A. D., 2016, MNRAS, 458, 4368
Milone A. P. et al., 2017, MNRAS, 465, 4363
Ngeow C.-C., Kanbur S. M., Neilson H. R., Nanthakumar A., Buonaccorsi J., 2009, ApJ, 693, 691
Persson S. E., Madore B. F., Krzemiński W., Freedman W. L., Roth M., Murphy D. C., 2004, AJ, 128, 2239
Pietrinferni A., Cassisi S., Salaris M., Castelli F., 2004, ApJ, 612, 168
Pietrinferni A., Cassisi S., Salaris M., Castelli F., 2006, ApJ, 642, 797
Piotto G., 2009, in Mamajek E. E., Soderblom D. R., Wyse R.F. G., eds, Proc. IAU Symp. Vol. 258. The Ages of Stars. Cambridge Univ. Press, Cambridge, p. 233
Piotto G. et al., 2007, ApJ, 661, L53
Raimondo G., 2009, ApJ, 700, 1247
Raimondo G., Brocato E., Cantiello M., Capaccioli M., 2005, AJ, 130, 2625
Renzini A., Buzzoni A., 1986, in Chiosi C., Renzini A., eds, Astrophysics and Space Science Library Vol. 122, Spectral Evolution of Galaxies. Reidel Publ. Co., Dordrecht, p. 195
Ripepi V. et al., 2012, MNRAS, 424, 1807
Romaniello M. et al., 2008, A&A, 488, 731
Rubele S. et al., 2012, A&A, 537, A106
Saha A., Sandage A., Tammann G. A., Dolphin A. E., Christensen J., Panagia N., Macchetto F. D., 2001, ApJ, 562, 314
Salpeter E. E., 1955, ApJ, 121, 161
Sasselov D. D. et al., 1997, A&A, 324, 471
Soszynski I. et al., 2008, Acta Astron., 58, 163
Stellingwerf R. F., 1982, ApJ, 262, 330
Storm J., Carney B. W., Gieren W. P., Fouqué P., Latham D. W., Fry A. M., 2004, A&A, 415, 531
Storm J. et al., 2011, A&A, 534, A95
Tanvir N. R., 1999, in Heck A., Caputo F., eds, Astrophysics and Space Science Library, Vol. 237, Post-Hipparcos Cosmic Candles. Kluwer Academic Pub., Dordrecht, p. 17
Udalski A., 2000, Acta Astron., 50, 279
Udalski A., Szymanski M., Kubiak M., Pietrzynski G., Soszynski I., Wozniak P., Zebrun K., 1999, Acta Astron., 49, 201
Udalski A. et al., 2008, Acta Astron., 58, 329
Ventura P., Zeppieri A., Mazzitelli I., D'Antona F., 1998, A&A, 334, 953
Ventura P., Castellani M., Straka C. W., 2005, A&A, 440, 623
Zaritsky D., Gonzalez A. H., Zabludoff A. I., 2004, ApJ, 613, L93

This paper has been typeset from a TEX/LATEX file prepared by the author.